Powder Metallurgy T15 Tool Steel: Part I. Characterization of Powder and Hot Isostatically Pressed Material

K.S. KUMAR, A. LAWLEY, and M.J. KOCZAK

The microstructure and constitution of T15 tool steel processed from gas-atomized powder have been characterized. From the atomized powder, four particle size ranges (≤840, 250 to 840, 44 to 100, and ≤44 μm) were consolidated to full density by hot isostatic pressing ("hipping") at 1130 °C or 1195 °C. Both atomized powder and consolidated material were examined by means of optical and electron microscopy, X-ray diffraction, chemical analysis, and microhardness. A segregated structure exists in the gas-atomized powder, independent of particle size; MC and M_2C carbides are present, primarily at cell boundaries. The matrix of the powders is a mix of martensite and retained austenite. Weight fraction and overall composition of the carbides are insensitive to particle size, but the proportion of MC carbides increases with decreasing particle size. After consolidation, MC, M_6C, and $M_{23}C_6$ carbides are present in a ferrite matrix. The carbide size distribution is skewed to larger carbide sizes at the higher consolidation temperature, independent of the prior particle size fraction, but there is no significant change in carbide volume fraction. For a given consolidation temperature, the size distribution of the MC and M_6C carbides is broader for the coarser particle size fractions.

I. INTRODUCTION

THE structure of ingot metallurgy (IM) high-speed steels has been investigated and reviewed extensively over the past 50 years.[1–13] In particular, the types and amounts of phases present have been determined as a function of composition and processing history. Typically, as-cast high-speed steels exhibit a microstructure consisting of coarse primary carbides in a matrix of ferrite. Subsequent hot working breaks up the coarse segregated carbides, but they remain clustered and exist as stringers in the working direction. The types of carbides present depend on composition and heat treatment.

Inhomogeneity in microstructure is reflected in distortion of the steel on austenitizing and quenching and in anisotropy in strength and toughness in the fully heat-treated condition. The coarse carbides resulting from slow cooling of these alloys with a large freezing range adversely affect properties such as strength, toughness, grindability, and tool life. To optimize mechanical properties and performance, it is necessary to control both the size and the distribution of the carbides.

Powder metallurgy (PM) high-speed steels have been a commercial reality for nearly 20 years.[14–17] Powder metallurgy processing involving the production of prealloyed powder by gas atomization, followed by consolidation to full density by hot isostatic pressing ("hipping"), mitigates the problems inherent to IM. Thus, the extent of segregation in PM tool steels is limited by the size of the powder particles, since each particle is a mini-ingot. On consolidating these powders, a fine homogeneous microstructure is achieved with accompanying improvement in strength, toughness, out-of-roundness distortion, grindability, and tool life, compared to IM tool steels of similar composition. Carbide size in consolidated PM tool steels is in the range of 0 to 3 μm, compared to a size range of 0 to 35 μm in IM tool steels.[18,19]

In gas-atomized powders, a range of powder particle size exists (≤1200 μm in gas-atomized commercial high-speed steels), and this implies a range of cooling rates. In general, it is accepted that with decreasing particle size, the cooling rate increases. Since the structure of high-speed steel is extremely sensitive to cooling rate,[20,21,22] it is clear that a spectrum of microstructures is present in commercial high-speed tool steel powders prior to consolidation.

The goal of this study has been to (1) assess the effect of cooling rate on powder particle microstructure, (2) characterize microstructural changes accompanying hipping to full density, and (3) determine the effect of heat treatment on the microstructure and mechanical properties of a T15 PM tool steel. This article is concerned with the first two goals. The third goal is the subject of a second article (Part II).[23]

II. EXPERIMENTAL PROCEDURE

A. *Processing*

T15 high-speed tool steel was atomized by Crucible, Inc., Pittsburgh, PA. The alloy charge was melted in a nitrogen atmosphere and nitrogen gas atomized. Powder was collected in liquid nitrogen at the base of the atomizing unit. Chemical analysis of the powder is summarized in Table I. Typical compositions for the corresponding commercial alloy powder and the IM counterpart are included in Table I for purposes of comparison. The three size fractions examined in powder form are given in Table II.

Cylindrical powder compacts (25.4 mm in diameter ×

K.S. KUMAR, Senior Scientist, is with Martin Marietta Laboratories, Baltimore, MD 21227. A. LAWLEY and M.J. KOCZAK, Professors, are with the Department of Materials Engineering, Drexel University, Philadelphia, PA 19104.

Manuscript submitted January 15, 1991.

Table I. Composition of Powder Metallurgy T15 High-Speed Tool Steel (Weight Percent)

Alloy Form	C	Cr	Co	W	V	Mo	Mn	Si	O	N
Powder/this study	1.52	4.67	5.22	12.19	4.85	—	0.31	0.46	0.0063	0.1
Powder/commercial	1.48	4.00	4.59	12.12	4.65	0.58	0.32	0.42	0.008	0.057
Ingot/commercial	1.57	4.62	5.10	13.59	4.86	0.69	0.30	0.21	—	—

152.4 mm in height) were outgassed, sealed under vacuum, and hipped at 1130 °C (code H1) or 1195 °C (code H2) under a pressure of 104 MPa. Four size fractions of powder were consolidated in this study (Table II). The higher of the two hipping temperatures (H2) is the temperature used by Crucible, Inc., for commercial PM T15. The lower temperature (H1) was examined as a possible means for improved control of carbide size and grain size during hipping.

B. *Microstructural Characterization*

T15 powder corresponding to different size fractions was examined by scanning electron microscopy (SEM) in order to characterize overall powder shape and surface condition. Mounted, polished, and etched powder cross sections from the three size fractions were examined by SEM and their microhardness determined.

The three powder size fractions were characterized in terms of the phases present using X-ray diffraction. Subsequently, the carbides in the powders were chemically extracted by dissolving away the matrix in a solution of phosphoric acid and water (ratio 2:1). X-ray diffraction patterns (diffractometry and Debye-Scherrer) of the carbide extracts were obtained using Cr-K_α or Cu-K_α radiation. Selective etching techniques were used to supplement the X-ray diffraction data. The weight fraction of carbides in each size fraction was evaluated using the cited extraction technique. Quantitative data for the elements present in the extracted carbides were obtained using chemical analysis.

In the hipped material, the matrix phase and the electrolytically extracted carbides[24] were characterized by means of X-ray diffraction. Microstructures were characterized by means of optical microscopy and SEM; this included selective etching to aid in the unambiguous determination of the carbides present in the hipped samples. M_6C-type carbides were selectively etched using a $KMnO_4$ + NaOH solution, and the MC carbides were electrolytically etched using a chromic acid solution. Volume fractions of MC and M_6C carbides and their accompanying size distributions were obtained by means of quantitative metallography utilizing a LEITZ* texture analysis system (TAS). The TAS is an image analyzer which optically scans the sample and provides data accumulated over 25 fields of view; each field covers an area of 4679 μm^2.

*LEITZ is a trademark of E. Leitz, Inc., Rockleigh, NJ.

Table II. Powder Size Fractions

Examined in Powder Form	Examined after Hipping
550 to 700 μm	<840 μm
110 to 130 μm	250 to 840 μm
<37 μm	44 to 100 μm
—	< 44 μm

III. RESULTS

A. *Atomized Powder*

Representative micrographs (SEM) of atomized powders in the three size ranges are shown in Figures 1(a) through (c). Typically, the particles are spherical in shape with relatively smooth surfaces. In each size fraction, small satellites are present.

In Figures 2(a) through (g), representative micrographs (SEM) of polished and etched powder cross sections are shown for the three size fractions. In the 550 to 700 μm size fraction, a segregated structure is evident and is characterized by a discontinuous network of carbides (Figure 2(a)). The rectangular area outlined in Figure 2(a) is shown at a higher magnification in Figure 2(b); plates of martensite are visible in the matrix.

Microstructures of the 110 to 130 μm size fraction powders are illustrated in Figures 2(c) and (d). The structure is similar to that in Figure 2(a) but is on a finer scale; also, the carbide network is more continuous than in the coarser size fraction (*cf.* Figures 2(a) and (c)). In several locations, particularly at the junction of three cells, the carbide structure has a morphology characteristic of eutectic solidification (Figures 2(b) and (d)). This is often referred to as a "script-carbide" morphology.

Representative microstructures of the <37 μm powder are illustrated in Figures 2(e) through (g). A wide range of particle sizes is present, and this is reflected in differing degrees of microstructural refinement (*cf.* Figures 2(e) and (f) and Figures 2(f) and (g)). In all cases, however, a segregated structure exists.

From a determination of the interplanar spacings and relative intensities in the three size fractions by X-ray diffraction, the matrix was identified as a mixture of a body-centered cubic (bcc) phase and a face-centered cubic (fcc) phase. The latter was identified as retained austenite. The bcc phase could not be unambiguously identified as α ferrite, δ ferrite, or martensite. The MC carbides were also present.

Based on interplanar spacings and relative intensities, the extracted carbides were identified as cubic MC and hexagonal M_2C. The proportion of M_2C carbides in the extracts decreased with decreasing particle size. This trend was also observed in the X-ray diffraction patterns for the three size fractions (Figure 3). The variation in the MC carbide lattice parameter as a function of particle size is shown in Figure 4. The particle sizes cover the range of 37 to 1200 μm. The lattice parameter decreased with decreasing particle size in the atomized powder. After

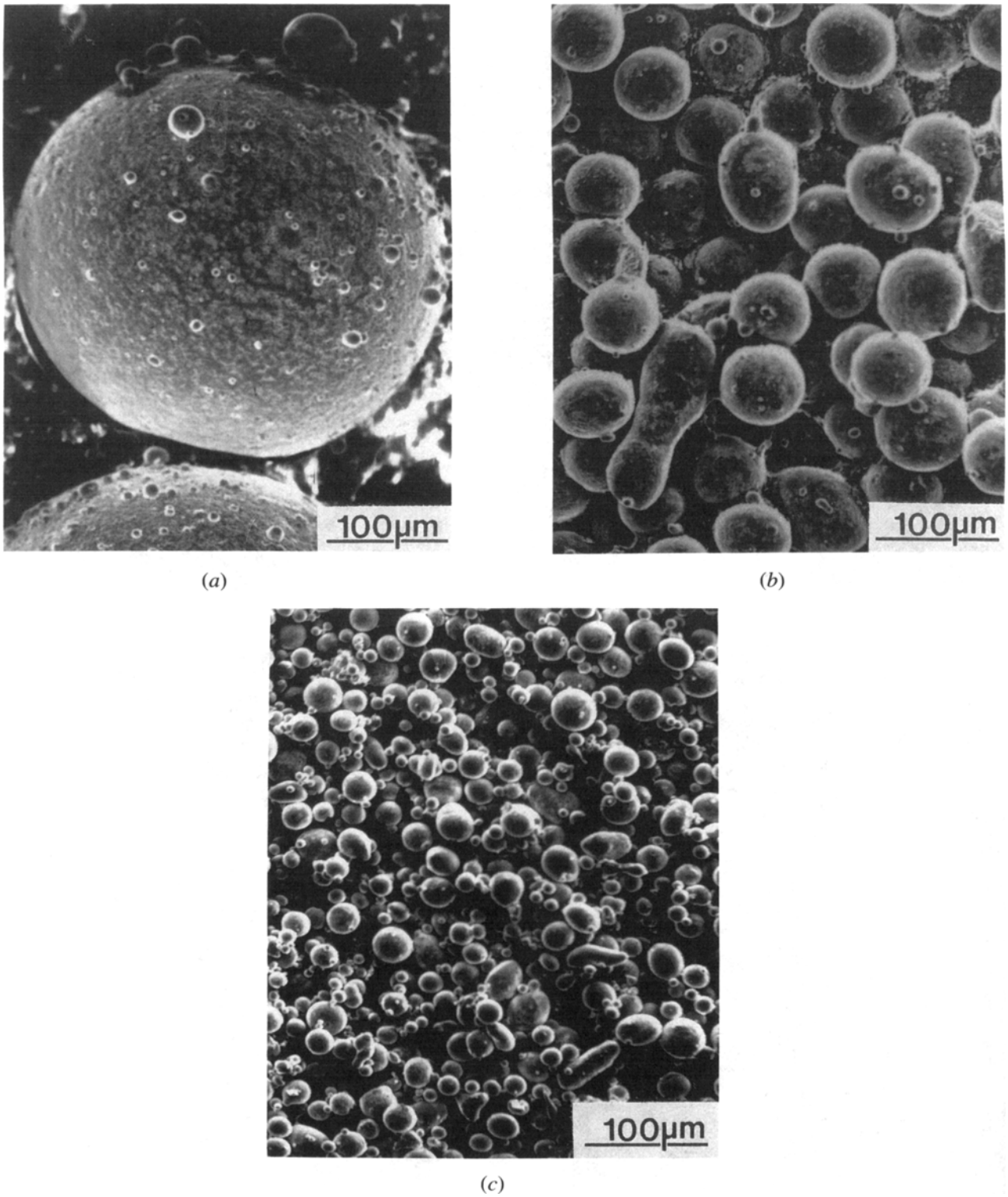

(*a*) (*b*) (*c*)

Fig. 1—As-atomized powder, SEM: (*a*) 350 to 420 μm, (*b*) 63 to 74 μm, and (*c*) ≤37 μm.

annealing the powder at 1130 °C for 1 hour, the variation in lattice parameter with particle size was nearly eliminated.

Weight fractions of the carbides (*i.e.*, the aggregate of MC and M_2C) in the three size fractions are summarized in Table III. The limits of experimental error were too high to observe any correlation between carbide content and powder particle size. For the three size ranges, the weight percents were in the range of 11.0 to 14.0 pct. The weight fraction of carbides in a quenched conventional IM T15 tool steel[2] is given for comparison.

Matrix and extracted carbide compositions, as determined by wet chemical analysis, are summarized in Table IV. The composition of the matrix was calculated

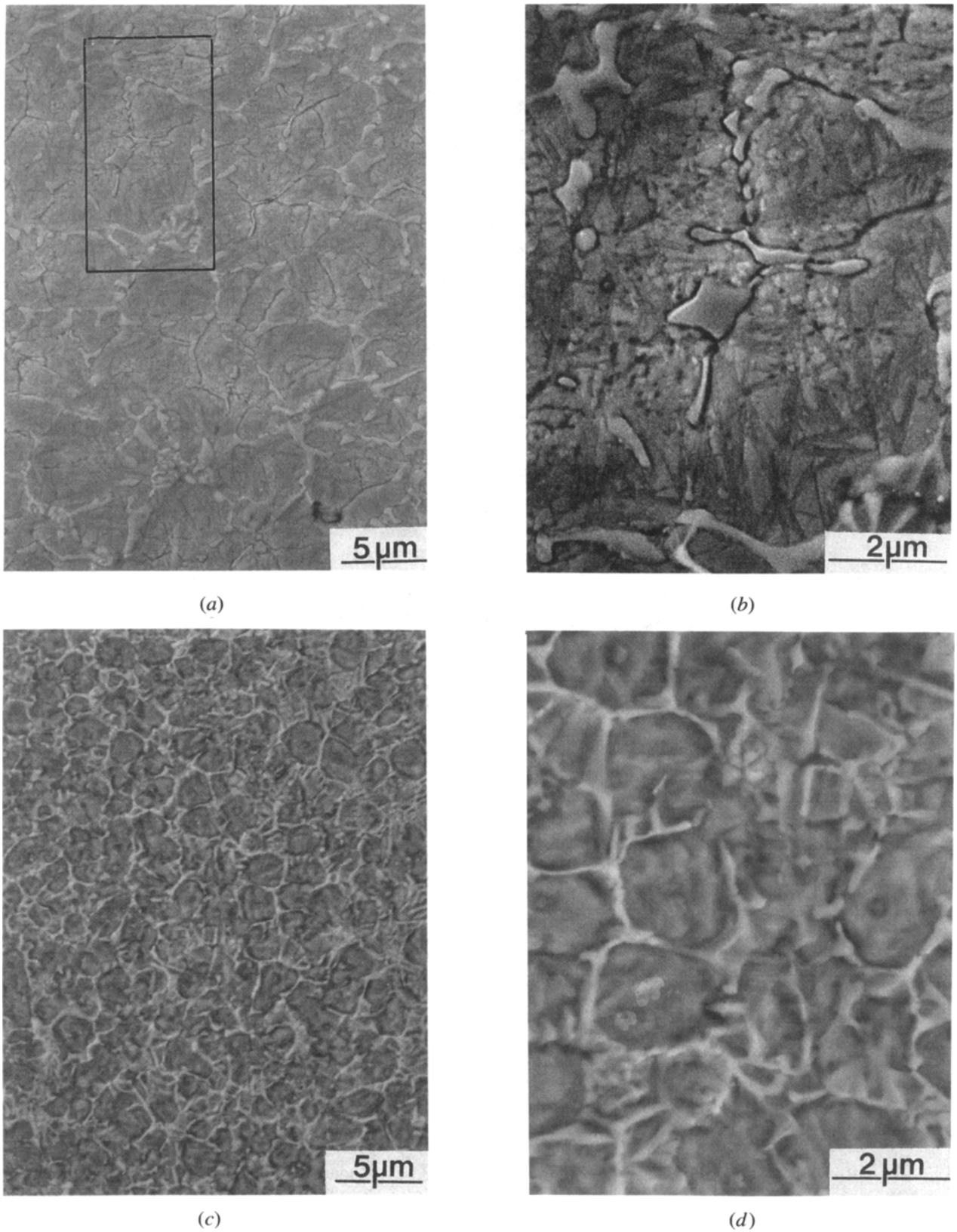

(*a*) (*b*) (*c*) (*d*)

Fig. 2—As-atomized powder, Kalling's etch, SEM: (*a*) and (*b*) 550 to 700 μm; (*c*) and (*d*) 110 to 130 μm; and (*e*) through (*g*) ≤37 μm.

from the composition of the carbides and the weight fraction of the carbides. No significant variation in carbide composition was observed with decreasing particle size. For the three size fractions evaluated, the carbides are rich in tungsten and vanadium, and the proportions of tungsten and vanadium in the carbides are insensitive to particle size. The amounts of chromium and carbon in the carbides increase with decreasing particle size. The matrix composition shows very little tungsten and vanadium; however, since the matrix comprises about

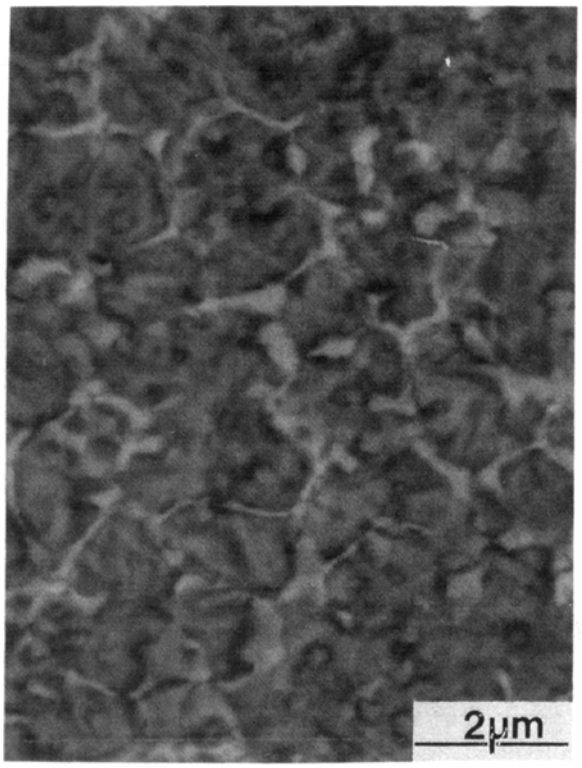

(e)

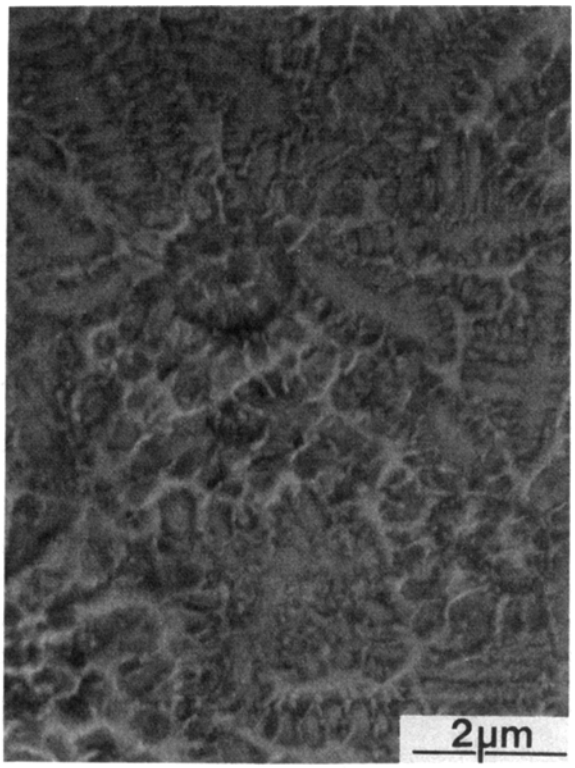

(f)

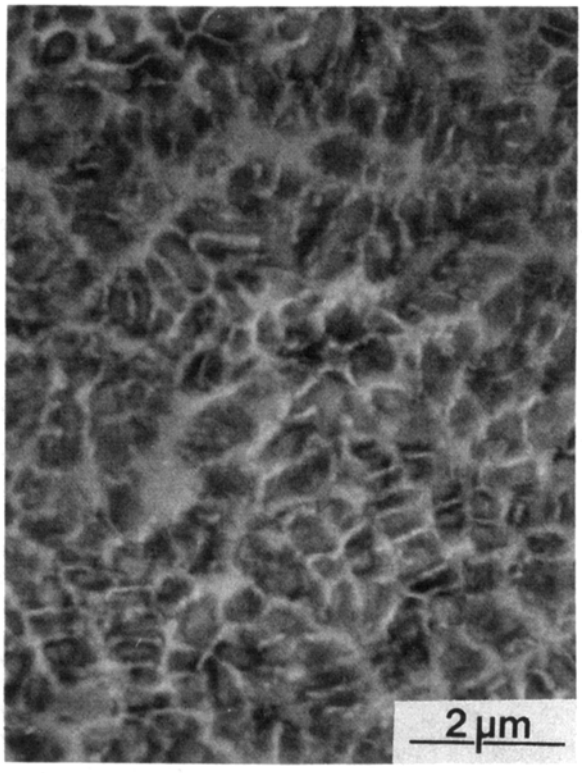

(g)

Fig. 2 Cont. — As-atomized powder, Kalling's etch, SEM: (*a*) and (*b*) 550 to 700 μm; (*c*) and (*d*) 110 to 130 μm; and (*e*) through (*g*) ≤37 μm.

88 wt pct of the alloy, about half of the tungsten is partitioned into the matrix. A similar argument holds for the vanadium. Most of the cobalt and significant amounts of chromium are present in the matrix. For purposes of comparison, the compositions of the carbides and the matrix in a quenched IM conventional T15 tool steel[2] are given.

Using a combination of scanning transmission electron microscopy and energy-dispersive X-ray analysis, Karagöz *et al.*[25] have quantitatively characterized the

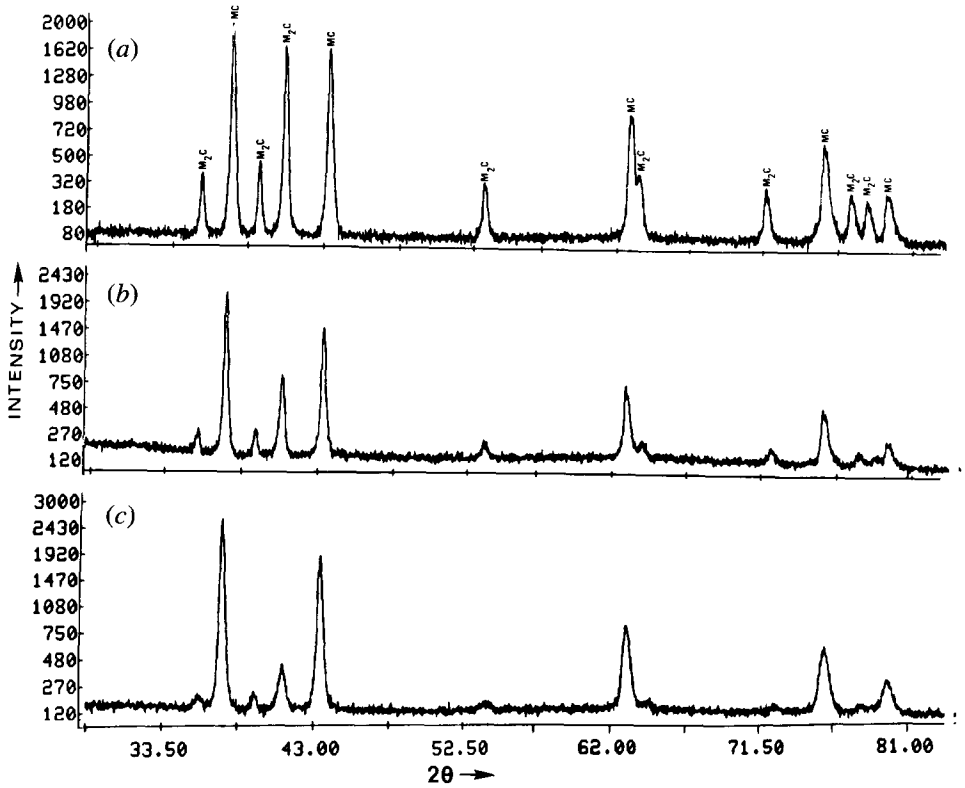

Fig. 3—X-ray diffraction traces of carbides extracted from atomized powder: (*a*) 550 to 700 μm screen, (*b*) 110 to 130 μm screen, and (*c*) ≤37 μm screen.

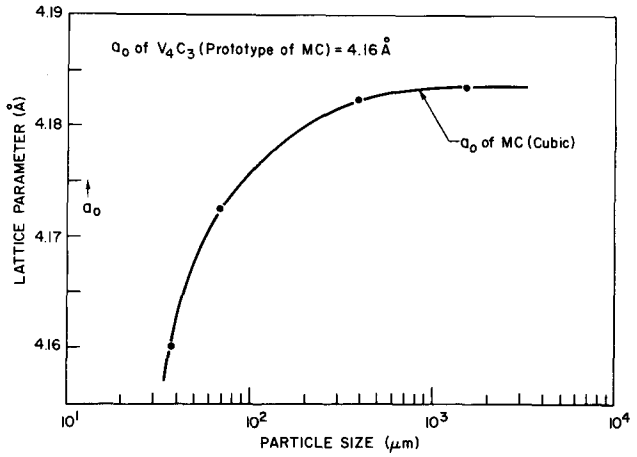

(*a*)

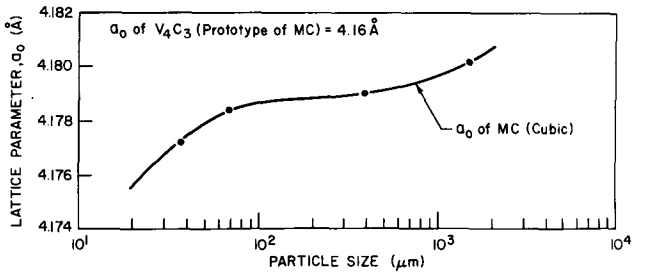

(*b*)

Fig. 4—Lattice parameter of MC carbides as a function of particle size in (*a*) the atomized powder and (*b*) after annealing at 1130 °C.

matrix and blocky carbides in several IM high-speed steels. This approach appears attractive for the determination of the composition of the fine carbides in PM tool steels, but specimen preparation is difficult. To date, we have not been able to prepare satisfactory electron-transparent foils from the ≤37 μm powder particles which contain extremely fine carbides.

In the absence of an independent analytical procedure with which to verify the present data, it is not known how completely the carbides are separated from the matrix in the atomized powder particles using chemical extraction.

Microhardness data for the atomized powder are given as a function of particle size in Figure 5. It is clear that microhardness increases with decreasing particle size.

B. *Consolidated Material*

Representative micrographs (SEM) of the two size fractions (250 to 840 μm and <44 μm) of the hipped material (H1 and H2) are shown in Figure 6. The carbides are coarser following hipping at the higher temperature (H2). For a given hipping temperature (H1 or H2), the carbide size is essentially independent of prior particle size fraction.

From X-ray diffraction analysis, it was found that in all cases, the matrix of the hipped material was α-ferrite. Debye-Scherrer analysis of the carbides extracted from the matrix confirmed the presence of cubic MC carbides, cubic M_6C carbides, and cubic $M_{23}C_6$ carbides, independent of the prior particle size fraction and hipping temperature.

Table III. Weight Fraction of Carbides* in T15 Atomized Powders

Size Fraction	Weight of Powder (g)	Weight of Carbides (g)	Carbide Content (Wt Pct)	Average Carbide Content (Wt Pct)
550 to 700 μm	(1) 25.20	3.262	12.94	12.93
	(2) 27.057	3.498	12.93	
110 to 130 μm	(1) 25.20	3.138	12.45	11.80
	(2) 25.122	2.800	11.15	
≤44 μm	(1) 25.05	3.509	14.01	13.50
	(2) 24.776	3.221	13.00	
Conventional** IM T15 austenitized (1250 °C) and oil quenched	—	—	—	12.4

*Aggregate MC and M_2C
**From Ref. 2.

Table IV. Partitioning of Alloying Elements between Matrix and Carbides* in Atomized T15 Powders

	Composition of Carbides (Wt Pct)						Composition of Matrix (Wt Pct)					
Size Fraction	W	V	Fe	Cr	Co	C	W	V	Fe	Cr	Co	C
500 to 700 μm	48.41	31.97	5.22	5.91	0.22	8.26	6.81	0.82	80.52	4.49	5.96	0.52
110 to 130 μm	48.45	31.36	4.70	6.80	0.15	8.54	7.34	1.30	79.62	4.39	5.90	0.58
≤44 μm	47.61	31.10	4.61	7.80	0.16	8.72	6.67	0.75	81.11	4.18	6.01	0.40
Conventional T15** austenitized (1250 °C) and oil quenched	47.2	29.8	8.7	2.9	1.0	9.1	7.3	1.4	81.2	5.1	4.3	0.40

Matrix composition calculated based on $M_p = M_c X_c + M_m(1 - X_c)$ where M_p = fraction of alloying element in the powder; M_c = fraction of alloying element in the carbide; M_m = fraction of alloying element in the matrix; and X_c = weight fraction of carbide in the powder.
*Aggregate MC and M_2C
**From Ref. 2.

Carbide volume fractions as a function of prior particle size fraction and hipping temperature, determined by quantitative metallography of selectively etched samples, are compared in Table V. The variations in volume fraction of the MC and M_6C carbides are less than the associated error bands, thereby precluding the identification of any trends.

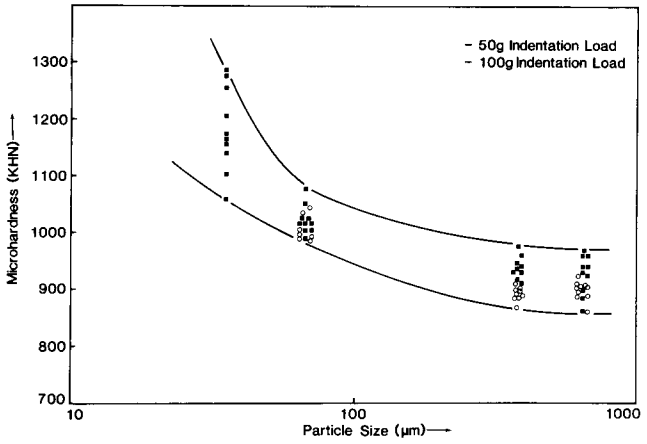

Fig. 5—Microhardness of atomized powder as a function of particle size.

On a volume basis, carbide size distributions are given in Table VI. The size distribution is displaced to larger carbide sizes with an increase in hipping temperature. The extent of the shift is greater for the M_6C carbides than for the MC carbides. For a given hipping temperature, the size distributions of MC and M_6C are somewhat dependent on the prior particle size fraction. The size distribution is broader in the coarse size fraction.

Size distribution data on a number basis are summarized in Table VII for the hipped material. From the table, it is seen that the effect of prior particle size fraction on carbide size distribution is more pronounced for the MC carbides than it is for the M_6C-type carbides. For both hipping temperatures (H1 and H2), the volume fraction of MC carbides in the 0 to 0.6 μm size range is higher in the ≤44 μm powder size fraction. The differences in the volume fraction of MC carbides in this size range between the coarse and fine powder screens are small. Corresponding differences considered on a number basis, however, are large because of the fineness of this size range. Quantitative evaluations in this size range are associated with a degree of uncertainty because of limitations in resolving the small particles.

A reliable selective etching technique for the unambiguous quantitative identification of $M_{23}C_6$ is not available to date. It has been established that this carbide,

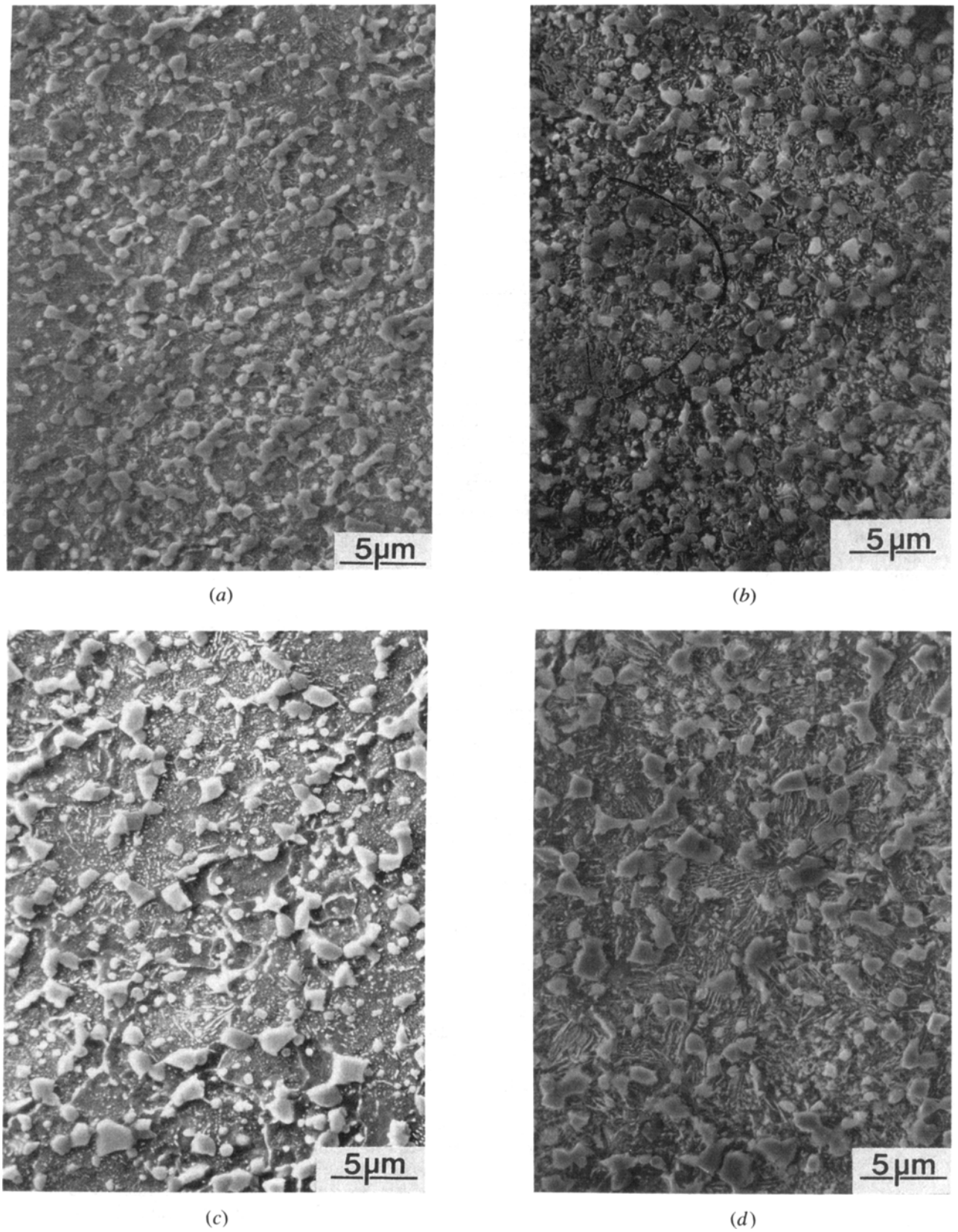

Fig. 6—Hipped material, Kalling's etch, SEM: (*a*) (H1)/250 to 840 μm screen, (*b*) (H1)/≤44 μm screen, (*c*) (H2)/250 to 840 μm screen, and (*d*) (H2)/≤44 μm screen.

Table V. Carbide Volume (Percent) as a Function of Powder Size Fraction and Hipping Temperature

Size Fraction	Carbide Type	H1	H2
250 to 840 μm	MC	16.2 ± 1.8*	17.9 ± 2.2
≤44 μm	MC	14.4 ± 1.2	14.1 ± 1.3
250 to 840 μm	M_6C	16.7 ± 3.7	16.6 ± 2.2
≤44 μm	M_6C	17.5 ± 1.5	15.2 ± 3.3

*Error band

which precipitates during the hipping cycle, constitutes ~10 vol pct in annealed IM T15.[2]

IV. DISCUSSION

A. *Atomized Powder*

In gas atomization, a stream of liquid metal is broken up by means of high-pressure gas jets. The resulting liquid droplets spheroidize in free fall, due to surface tension, before solidification. Particle collisions can occur before and/or after solidification, and this is responsible for satellite formation. Ligaments are observed in the finer size fractions (*cf.* Figures 1(a) with 1(b) and 1(b) with 1(c)), and their presence can be explained on the basis of the mechanism of droplet formation in gas atomization and the decrease in solidification time with decreasing particle size.[26]

In the atomized powder, the solidification sequence is envisaged as the primary nucleation of austenite from the liquid followed by the precipitation of proeutectic MC carbides, together with austenite along the cell walls. Subsequently, eutectic decomposition of the solute-enriched liquid occurs over a range of temperatures, into austenite, MC, and M_2C carbides at the junctions of three cells (Figures 2(a) and (c)).

Tool steels with their high alloy content exhibit a large freezing range; thus, it is unlikely that particles in gas atomization are undercooled sufficiently to permit diffusionless solidification. Solidification will commence and proceed in the liquid- plus solid-phase fields with the formation of alloy-lean dendrites and the rejection of solute, including carbon, into the liquid. In consequence, microstructural refinement observed as a function of particle size arises primarily from differences in the growth process, as the time for coarsening during solidification is reduced in the finer particles (*cf.* Figures 2(a) and (c)). This inference is also supported by the fact that the carbide content and the matrix composition were similar for the different size fractions (Tables III and IV).

It is interesting to note that the carbide weight percent and the matrix composition of austenitized and quenched IM T15[2] were similar to those of the atomized powders used in this study (Tables III and IV). The higher level

Table VI. MC and M_6C Size Distribution (Volume Basis) in Hipped Material

Size Fraction	Processing Code	Carbide Type	Total Carbide (Vol Pct)	Volume Fraction in Given Size Range (μm)					
				0 to 0.6	0.6 to 1.2	1.2 to 1.8	1.8 to 2.4	2.4 to 3.0	>3.0
Coarse*	H1	MC	16.2	0.28	0.64	0.07	0.01	0.007	—
Coarse	H2	MC	17.9	0.10	0.50	0.36	0.03	0.003	—
Fine**	H1	MC	14.4	0.38	0.59	0.02	0.004	0.001	—
Fine	H2	MC	14.1	0.17	0.55	0.26	0.02	0.006	—
Coarse*	H1	M_6C	16.7	0.10	0.32	0.37	0.13	0.035	0.045
Coarse	H2	M_6C	16.6	0.07	0.18	0.36	0.28	0.09	0.02
Fine**	H1	M_6C	17.5	0.11	0.40	0.43	0.05	0.007	—
Fine	H2	M_6C	15.2	0.06	0.16	0.40	0.34	0.04	0.003

*250 to 840 μm
**<44 μm

Table VII. MC and M_6C Size Distribution (Number Basis) in Hipped Material

Size Fraction	Processing Code	Carbide Type	Number of Carbides in 25 Fields	Number Fraction in Given Size Range (μm)					
				0 to 0.6	0.6 to 1.2	1.2 to 1.8	1.8 to 2.4	2.4 to 3.0	>3.0
Coarse*	H1	MC	27,738	0.63	0.36	0.01	—	—	—
Coarse	H2	MC	18,257	0.39	0.47	0.14	0.006	—	—
Fine**	H1	MC	32,733	0.71	0.29	0.004	—	—	—
Fine	H2	MC	19,449	0.53	0.39	0.08	0.003	—	—
Coarse*	H1	M_6C	14,490	0.50	0.34	0.14	0.02	0.003	—
Coarse	H2	M_6C	11,474	0.49	0.24	0.19	0.07	0.01	—
Fine**	H1	M_6C	16,554	0.45	0.39	0.16	0.01	—	—
Fine	H2	M_6C	10,411	0.44	0.23	0.22	0.11	0.007	—

*250 to 840 μm
**<44 μm

of iron and the lower level of chromium in the carbides in the austenized and quenched IM T15 are explained by (1) the presence of M_6C carbides, which have a significant level of solubility for iron, (2) the absence of M_2C carbides which have low solubility for iron but dissolve chromium to appreciable levels, and (3) the complete dissolution of chromium-rich $M_{23}C_6$ carbides. In the atomized powder, M_6C carbides are not present but MC and M_2C carbides are present; hence, the low iron and high chromium content of these elements in the carbides extracted from the powders.

The matrix was identified as a mixture of a bcc phase and retained austenite. The bcc phase suggests the presence of martensite and/or δ-ferrite in addition to the retained austenite. Tetragonality was not detected in the X-ray diffraction pattern of the bcc phase, but this is not unexpected, since the broadness of the diffraction lines and merging of doublets obscure the tetragonality of martensite containing less than 0.6 wt pct C.[27] In atomized powders, line broadening arising from lattice strains and fine structures will enhance the broadening from the martensite.

Steven *et al.*[28] have shown that in 18W-4Cr-1V tool steel, δ-ferrite nucleates first on solidification. On increasing the carbon content above 1.1 wt pct, δ-ferrite is not formed; instead, austenite is the primary phase to nucleate from the liquid during solidification. Based on the above observation, the bcc product observed in the matrix of the atomized powder is likely to be martensite rather than δ-ferrite; further, plates of martensite were identified in the coarse size fraction (Figure 2(b)). The presence of retained austenite in the atomized powder is the result of a low M_s temperature due to the high levels of carbon, chromium, and the other alloying elements trapped in the matrix due to rapid quenching following solidification. Quenching in liquid nitrogen results in the formation of a gas film around the particles, which causes a decrease in the quenching rate and, consequently, "stabilization" of the austenite.[11] Cohen *et al.* found 8 wt pct retained austenite on quenching austenitized IM T1 high-speed steel in liquid nitrogen.[11]

X-ray diffraction analyses of carbides extracted from the atomized powders confirmed the presence of MC and M_2C-type carbides and the absence of M_6C-type carbides in the size fractions evaluated. On annealing, M_2C carbides decompose and yield MC, M_6C, and $M_{23}C_6$ carbides in a matrix of α-ferrite. This implies that M_2C carbides are metastable and form only in the atomized powder.

Sare and Honeycombe[21] attribute the presence of M_2C in splat-quenched M1 tool steels to the high concentration of carbon in solution. This broadens the composition and temperature range over which M_2C can form. On aging these splats, both MC and M_2C carbides were observed. Overaging led to the precipitation of M_6C carbides. Brandis *et al.*[5] claim that the types of carbides precipitating during solidification are dependent primarily on the composition of the steel. While elements such as vanadium and niobium form MC carbides, tungsten, silicon, and nitrogen stabilize M_6C-type carbides. M_2C-type carbides are stabilized by molybdenum, carbon, and vanadium. The solidification rate influences the types of carbides that precipitate; a higher cooling rate favors the precipitation of M_2C over M_6C. Nitrogen combines with vanadium and carbon to form vanadium carbonitrides, thereby consuming a greater portion of vanadium, which is essential in the formation of M_2C carbides; as a consequence, M_6C is stabilized.[5]

The presence of M_2C carbides in the atomized powder is attributed to the attendant rapid cooling, to the extent that M_2C carbides are favored over M_6C carbides at high solidification rates. Further, the presence of vanadium in the solute-enriched liquid in the mushy particle aids in the formation of M_2C carbides. Although the total carbide content is insensitive to the powder particle size, the relative amounts of MC and M_2C are not; the proportion of M_2C carbides decreases with decreasing particle size. This decrease in M_2C carbide content is attributed to the differences in proeutectic MC carbide composition as a function of powder particle size. The difference in carbide composition arises because of the different levels of undercooling experienced by the coarse and fine powders. Fine particles contain a lesser number of potential heterogeneous nucleation sites and therefore experience a higher degree of undercooling. If it is assumed that during solidification the relative amounts and compositions of the coexisting phases are those given by the phase diagram, then the solidification path followed by the coarse particles will differ from that followed by the fine powder. This is due to the fact that solidification commences at different temperatures for the two powder screens. Thus, it is envisaged that the proeutectic MC carbides in the coarse size fraction are richer in vanadium (with some tungsten dissolved in them) than the fine size fraction. In the fine size fraction, the proeutectic MC carbides are thought to contain higher levels of tungsten. As a consequence, the coexisting liquid composition is different for the coarse and fine powders. Specifically, the composition of the liquid will be richer in tungsten for the coarse size fraction. Subsequently, the liquid in both the coarse and fine size fractions decomposes by a eutectic reaction to yield austenite, MC carbides, and M_2C carbides. The relative amounts of MC to M_2C will differ in the two cases, the ratio M_2C:MC being greater for the coarse size fraction than for the fine size fraction. A schematic of the envisaged solidification process for the coarse as well as the fine size fractions is shown in Figure 7. Insensitivity in the tungsten and vanadium content in the carbides as a function of particle size (Table IV) is attributed to a combination of two factors: (1) the partitioning of these alloying elements between the MC and M_2C carbides and (2) the variations in the relative proportions of MC and M_2C carbides as a function of particle size. Karagöz *et al.*[25] have shown that depending on solidification history, certain carbides exhibit a wide variation in composition.

A high-temperature isotherm of the ternary V-W-C system shows that W_2C and V_2C exhibit a continuous range of mutual solid solubilities with a hexagonal structure.[29] The lattice parameters of the W_2C carbide decrease with increasing vanadium content. Although MC carbides are vanadium-rich at room temperature, at elevated temperatures (1600 °C), they dissolve up to 40 at. pct tungsten. The VC carbides are cubic and exhibit a defect structure of the type VC_{1-x}. The lattice parameter

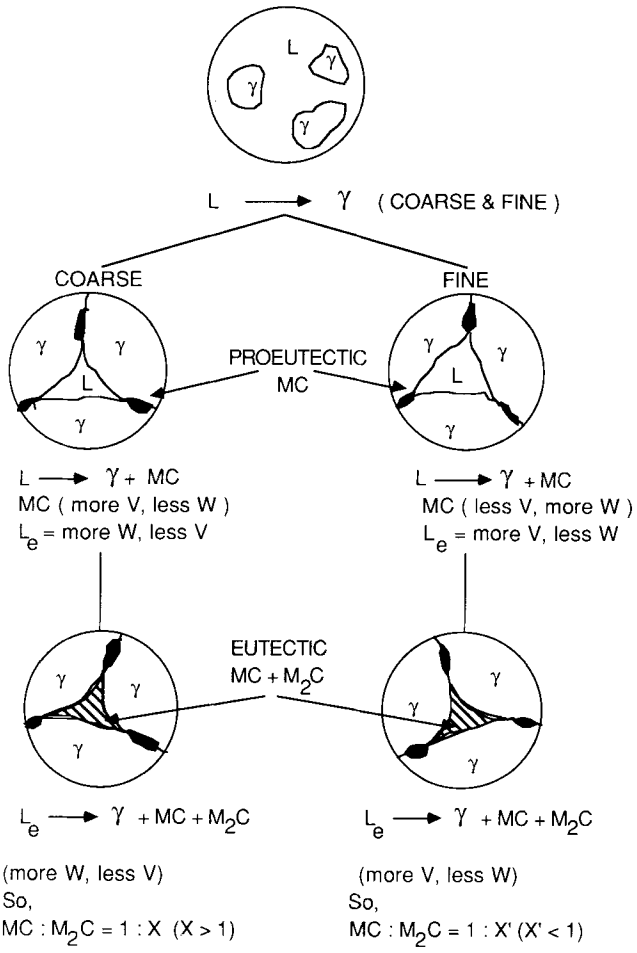

Fig. 7—Proposed solidification sequence for coarse and fine particles resulting from gas atomization (schematic).

of VC increases with increasing tungsten content for a fixed carbon content and decreases with decreasing carbon content for a fixed level of dissolved tungsten.[29]

The lattice parameter of MC decreases with decreasing particle size (Figure 4). Variations in MC carbide chemistry as a function of particle size, arising from substitutional alloying (*i.e.*, with tungsten and chromium), cannot account for the magnitude of the decrease observed. This implies that the carbon content of the MC carbides decreases with decreasing particle size. Carbon being an interstitial atom dilates the lattice more than a substitutional atom such as tungsten and therefore overshadows the effect of increasing tungsten content with decreasing particle size. A change of stoichiometry in the vanadium carbide from $VC_{0.79}$ to $VC_{0.85}$ increases the lattice parameter from 0.413 to 0.417 nm. To produce a similar increase in the lattice parameter, approximately 25 at. pct tungsten must be dissolved in $VC_{0.79}$ to form $(V, W)C_{0.79}$.[29] The gradual increase in carbon content in the carbides with decreasing particle size (Table IV) is associated with two opposing tendencies, (1) increasing proportion of MC to M_2C carbides with decreasing particle size and (2) decrease in carbon content of the MC carbides (defect structure) with decreasing particle size.

Calculations based on X-ray peak height measurements* show that the ratio of MC to M_2C carbides varies from 10:7 in the 550 to 700 μm size fraction, to 10:3 in the 110 to 130 μm size fraction, and to 10:1 in the $\leq$44 μm powder screen. The levels of carbon in the carbides for these three size fractions are 38.4 at. pct, 39.4 at. pct, and 39.7 at. pct, respectively. If it is assumed that M_2C does not exhibit a defect structure, calculation shows that the MC carbide structure varies from $MC_{0.839}$ in the coarse (550 to 700 μm) size fraction to $MC_{0.807}$ in the fine ($\leq$44 μm) size fraction. This results in a change of 0.032 in the carbon content. Based on previous observations and assuming that the lattice parameter varies linearly with carbon content in VC carbides, a change in MC from $MC_{0.839}$ to $MC_{0.807}$ must cause a decrease in lattice parameter by 0.002 nm. This is in agreement with the variation in the lattice parameter as a function of particle size (Figure 4).

*The intensity of a diffraction line depends on the atomic scattering factor, which, in turn, is approximately proportional to the atomic number. The presence of differing levels of tungsten (Z = 74) in these carbides will influence the intensity measurements.

The variation in microhardness with particle size is shown in Figure 5. For all of the powder size fractions examined, the hardness is extremely high. High-carbon high-alloy ferrous martensite exhibits a hardness of 750 KHN, while the lowest value recorded for the powders is much higher. This extremely high hardness arises from an interplay of the following factors: (1) highly alloyed austenite + martensite matrix, (2) fine microstructure in terms of grain size and carbide size, (3) transformation of retained austenite to martensite during hardness measurement, and (4) cellular morphology of the extremely hard fine-scale carbides.

With decreasing particle size, microhardness gradually increases, because the cell size decreases with decreasing particle size and because the proportion of the extremely hard MC carbides increases. The larger scatter in values observed for the $\leq$37 μm powder size is attributed to (1) variations in microstructure from particle to particle in this size fraction, (2) difficulty in obtaining an absolutely flat surface due to the fine powder size, and (3) difficulty in obtaining an adequate indentation area on each particle.

B. *Consolidated Material*

After hipping, MC, M_6C, and $M_{23}C_6$ carbides are present in a ferrite matrix. Slow cooling, inherent to the hipping cycle, leaves the consolidated material in the annealed condition, and these carbides are known to be present after annealing.[2]

For a particular hipping temperature, the carbides are approximately the same size for the coarse and fine powder size screens. The carbides are, however, coarser after hipping at the higher temperature (Figures 6(a) through (d)). The similarity in microstructure as well as in the volume fractions of MC and M_6C carbides in the coarse and fine size fractions after each hipping temperature (Table V) reflects the effectiveness of hipping in eliminating differences in the initial microstructure of the atomized powder. Since the volume fractions of MC and

M_6C carbides approach the room-temperature solubility of these carbides in the ferrite matrix, the volume fractions of these carbides are independent of the hipping temperature. The effect of different hipping temperatures, however, is reflected in the size distribution of the MC and M_6C carbides (Table VI and Table VII). The size distributions of the carbides are displaced to coarser sizes with increasing hipping temperature. The effect is more pronounced for M_6C carbides than MC carbides. During heating to the hipping temperature, both MC and M_6C carbides precipitate in the matrix. At higher temperatures and at the hipping temperature, a fraction of the MC and M_6C carbides go into solution, as dictated by the solubility of these carbides in the matrix at that temperature. A higher hipping temperature implies more dissolution of these carbides. In comparison to M_6C, very little MC dissolves because of the higher stability of MC. On slow cooling from the hipping temperature, these carbides precipitate because of a decrease in the matrix solubility level. The carbides can readily precipitate onto existing carbides, resulting in coarser carbides. The effect is therefore more pronounced for the material hipped at the higher temperature. This results in a displacement of the carbide size distribution to coarser sizes with a higher hipping temperature. The effect is more pronounced for the M_6C carbides.

The variation in carbide size distribution with prior particle size fraction is dependent on nucleation and growth. The presence of a narrower size spread of MC and, to a lesser extent, M_6C carbides in the fine size fraction ($\leq$44 μm) as compared to the coarse size fraction (250 to 840 μm) implies a higher number of nucleation events and restricted growth in the fine size fraction. Potential nucleation sites available during hipping include powder particle surfaces and inhomogeneities such as grain boundaries and cell walls. M_6C carbides precipitate from the matrix as well as from decomposition of the M_2C carbides present in the atomized powder. Further, tungsten rejected by the supersaturated MC carbides in the atomized powders also combines with the carbon available from the decomposition of the M_2C carbides and carbon from the matrix to form M_6C carbides. In the fine powder size fraction, there is more powder surface area per unit volume available for nucleation. The cell size in the finer powder size fraction is also smaller; thus, a large surface area of cell walls is available for the nucleation of MC and M_6C carbides. This results in a narrower size spread in the carbide sizes in the fine size fraction as compared to the coarser counterpart. During heating and at the hipping temperature, a significant amount of the M_6C carbides goes into solution, consistent with the solubility level of these carbides in the matrix at these temperatures. Since the stability of the MC carbides is greater than that of the M_6C carbides, significant dissolution of the former at the hipping temperature does not occur.

During cooling from the hipping temperature (H1 or H2), reprecipitation of M_6C carbides occurs on existing M_6C carbides, and this reduces the effect of the higher nucleation rate and restricted growth, a condition that was present in the finer powder size fraction. The end result is a marginal difference in the size distributions of M_6C carbides as a function of the prior particle size fraction for a fixed hipping temperature (*cf.* Tables VI and VII). Since very little MC goes into solution at the hipping temperature, only minor amounts of reprecipitation take place on cooling to room temperature. The presence of a higher number fraction of MC carbides in the 0 to 0.6 μm size range in the fine powder size fraction reflects the higher nucleation rate and restricted growth of these carbides in this powder size range.

V. CONCLUSIONS

1. Refinement in the scale of the microstructure with decreasing particle size and, therefore, higher cooling rates is attributed to restricted growth.
2. Solidification proceeds by the nucleation of austenite from the liquid phase followed by precipitation of proeutectic MC carbides and subsequent eutectic decomposition of the solute-enriched liquid over a range of temperatures into austenite, MC, and M_2C carbides.
3. The decrease in the proportion of M_2C carbides with decreasing particle size is attributed to the higher levels of undercooling in the finer particle sizes and their influence on the liquid composition and solidification process.
4. The compositions of the MC and M_2C carbides are influenced by the particle size and, hence, the solidification rate.
5. The ratio of metal to carbon atoms in the MC carbides increases with decreasing particle size. This is reflected in a decrease in lattice parameter of the MC carbide with decreasing particle size.
6. Microhardness of the powders increases with decreasing particle size.
7. From microstructural observations of the hipped material, it is concluded that any prior effect of particle size is eliminated during hipping.
8. For both hipping temperatures (H1 and H2), MC, M_6C, and $M_{23}C_6$-type carbide are present in a matrix of α-ferrite.
9. The volume fractions of MC and M_6C carbides are insensitive to the prior particle size fraction and/or hipping temperature.
10. The MC and M_6C carbide size distributions for the coarse and fine powder screens are displaced to coarser sizes for the higher hipping temperature.
11. For a particular hipping temperature, the fine powder screen exhibits a narrower spread of MC and, to a lesser extent, M_6C carbides than the coarse powder screen.

ACKNOWLEDGMENTS

This research was sponsored by the Office of Naval Research, Washington, DC (Contract No. N00014-84-K-0472). The authors are indebted to Dr. Donald E. Polk (Technical Liaison Officer) for interest and counsel. Acknowledgment is given to John Moll, Crucible Research Center, Pittsburgh, PA, for assistance with atomization and consolidation of the tool steel powder.

REFERENCES

1. D.J. Blickwede, M. Cohen, and G.A. Roberts: *Trans. ASM*, 1950, vol. 42, pp. 1161-96.
2. F. Kayser and M. Cohen: *Met. Prog.*, 1952, vol. 61 (6), pp. 79-85.
3. C.J. McHargue, J.P. Hammond, and C.S. Crouse: *Trans. ASM*, 1954, vol. 46, pp. 716-26.
4. J. Edwin Bridge, Jr., Gunvant N. Maniar, and Thoni V. Philip: *Metall. Trans.*, 1971, vol. 2, pp. 2209-14.
5. H. Brandis, E. Haberling, and H.H. Weigand: in *Processing and Properties of High-Speed Tool Steels*, M.G.H. Wells and L.W. Lherbier, eds., TMS-AIME, Warrendale, PA, 1980, pp. 1-18.
6. A.K. Seal and R.W.K. Honeycombe: *J. Iron Steel Inst.*, 1958, vol. 188, pp. 9-15.
7. H.J. Goldschmidt: *J. Iron Steel Inst.*, 1952, vol. 170, pp. 189-204.
8. T. Malkiewicz, Z. Bojarski, and J. Foryst: *J. Iron Steel Inst.*, 1959, vol. 193, pp. 25-31.
9. K. Kuo: *J. Iron Steel Inst.*, 1953, vol. 173, pp. 363-75.
10. K. Kuo: *J. Iron Steel Inst.*, 1957, vol. 185, pp. 297-303.
11. M. Cohen: *Trans. ASM*, 1949, vol. 41, pp. 35-95.
12. R.W. Balluffi, M. Cohen, and B.L. Averbach: *Trans. ASM*, 1951, vol. 43, pp. 497-517.
13. K. Kuo: *J. Iron Steel Inst.*, 1953, vol. 174, pp. 223-28.
14. E.J. Dulis: in *Powder Metallurgy for High Performance Applications*, J.J. Burke and V. Weiss, eds., Syracuse University Press, Syracuse, NY, 1972, pp. 317-29.
15. K. Zander: *Powder Metall. Int.*, 1970, vol. 2 (4), pp. 129-32 and 134.
16. H.F. Fischmeister: *Rev. Mater. Sci.*, 1975, vol. 5, pp. 151-76.
17. H. Takigawa, H. Manto, N. Kawai, and K. Homma: *Powder Metall.*, 1981, vol. 24 (4), pp. 196-202.
18. A. Kasak and E.J. Dulis: *Powder Metall.*, 1978, vol. 21 (2), pp. 114-21.
19. E.J. Dulis and T.A. Neumeyer: in *Progress Powder Metallurgy*, A.S. Bufferd, ed., MPIF, New York, NY, 1972, vol. 28, pp. 129-42.
20. H.F. Fischmeister, A.D. Ozerskii, and L. Olsson: *Powder Metall.*, 1982, vol. 25 (1), pp. 1-9.
21. I.R. Sare and R.W.K. Honeycombe: *Met. Sci.*, 1979, vol. 13, pp. 269-79.
22. J.J. Rayment and B. Cantor: *Metall. Trans. A*, 1981, vol. 12A, pp. 1557-68.
23. K.S. Kumar, A. Lawley, and M.J. Koczak: *Metall. Trans. A*, 1991, vol. 22A, pp. 2747-59.
24. D.J. Blickwede and M. Cohen: *Trans. TMS-AIME*, 1949, vol. 185, pp. 578-84.
25. S. Karagöz, I. Liem, E. Bischoff, and H.F. Fischmeister: *Metall. Trans. A*, 1989, vol. 20A, pp. 2695-2701.
26. J.B. See and G.H. Johnston: *Powder Technol.*, 1978, vol. 21, pp. 119-33.
27. I.R. Sare and R.W.K. Honeycombe: *J. Mater. Sci.*, 1978, vol. 13, pp. 1991-2002.
28. G. Steven, J.J. Hauser, T.A. Neumeyer, and J.M. Capenos: *Trans. ASM*, 1969, vol. 62, pp. 180-94.
29. W.B. Pearson: in *A Handbook of Lattice Spacings and Structures of Metals and Alloys*, G.V. Raynor, ed., Pergamon Press Ltd., New York, NY, 1967, vol. 2, p. 1397.